Journal of Experimental Nanoscience
Publication details, including instructions for authors and subscription information:
http://www.informaworld.com/smpp/title~content=t716100757

Recent advances in gene delivery with ultrasound and microbubbles

Chantal Pichon[a]; Kadija Kaddur; Patrick Midoux[a]; François Tranquart; Ayache Bouakaz
[a] Centre de Biophysique Moléculaire-UPR4301 CNRS, affiliated to University of Orléans and Inserm, France

To cite this Article Pichon, Chantal , Kaddur, Kadija , Midoux, Patrick , Tranquart, François and Bouakaz, Ayache(2008) 'Recent advances in gene delivery with ultrasound and microbubbles', Journal of Experimental Nanoscience, 3: 1, 17 — 40
To link to this Article: DOI: 10.1080/17458080801993422
URL: http://dx.doi.org/10.1080/17458080801993422

Journal of Experimental Nanoscience
Vol. 3, No. 1, March 2008, 17–40

Taylor & Francis
Taylor & Francis Group

Recent advances in gene delivery with ultrasound and microbubbles

Chantal Pichon[a]*, Kadija Kaddur[b], Patrick Midoux[a], François Tranquart[b] and Ayache Bouakaz[b]

[a]*Centre de Biophysique Moléculaire-UPR4301 CNRS, affiliated to University of Orléans and Inserm, Orléans, France;* [b]*Inserm, Tours, and Université F. Rabelais, Tours, France*

(*Received 3 August 2007; final version received 15 February 2008*)

Recently, microbubbles used in combination with ultrasound has been proposed as an alternative method for *in vitro* and *in vivo* gene delivery. Ultrasound (US) and microbubble assisted delivery (USMD) has great clinical potential based on the fact that ultrasound contrast agents (USCAs) are clinically approved for diagnostic applications. The mechanism that supports gene delivery *via* USMD is thought to be 'sonoporation'. It is hypothesised that the interaction of US and USCA can induce a transient cell membrane permeabilisation leading to enhanced DNA uptake. The exact mechanism(s) of gene uptake remains a subject of academic debate and various hypotheses have been proposed, including acoustic microstreaming or local shear stresses, microjetting and cavitation. This review provides the current understanding of USMD and highlights both the bubble characteristics and ultrasound parameters that support USMD *in vitro* and *in vivo*. Both safety and efficacy of gene delivery by sonoporation are discussed. In addition, USMD is compared with electroporation, another widely used physical method for gene delivery.

Keywords: sonoporation; contrast agent; gene transfer electroporation

1. Introduction

Gene therapy aims to introduce nucleic acids or genetic material into mammalian cells in order to modulate gene expression and to achieve therapeutic benefits. Although viral vectors have demonstrated the feasibility of this therapeutic approach and remain the best vehicles to introduce genes into cells, alternative approaches capable of safely delivering genes into cells both with high efficacy and low to minimal immunogenicity, remain a fundamental requirement. Indeed, despite successful clinical trials on ornithine carbamyltranscarbamylase deficiency and on Severe Combined X linked immunodeficiency, severe fatal adverse effects linked to the use of viral vectors have been reported [1–3]. Over the last decade, considerable attention has been paid to identifying and/or designing non-viral vectors, as alternative approaches to delivering

*Corresponding author. Email: chantal.pichon@cnrs-orleans.fr

ISSN 1745–8080 print/ISSN 1745–8099 online

DOI: 10.1080/17458080801993422
http://www.informaworld.com

genes. Among these, chemical gene delivery systems that incorporate viral-like features to transfect cells [4,5] have been reported. The final goal of these systems is to transform a plasmid DNA (pDNA) encoding a therapeutic gene into a 'magic bullet', suitable to deliver the desired gene into the right target cells and to transfer the gene in the nucleus upon systemic administration. This challenge will be achieved when the 'magic bullet' is able to cross several extracellular barriers (blood vessels and microvessels) before reaching the target cells and to pass through several intracellular barriers (intracellular membranes and compartments) to reach the target cell's nucleus where the gene expression takes place (Figure 1). On reaching the target cell, the plasma membrane is the first barrier that must be overcome. Since pDNA are negatively charged, they are hardly internalised by cells. Plasmid DNA can be taken up by cells *via* endocytosis if they are complexed with synthetic vectors. Once endocytosed, pDNA particles are usually confined inside endosomes or vesicles from where they must escape. Moreover, within the cytosol, molecule or particle diffusion is highly dependent on their size, although microtubules or actin microfilaments, components of the cytoskeleton, the molecular complex scaffold maintaining the cell architecture, could all be used as railways for cytosolic diffusion. pDNA should reach the nucleus where the expression machinery takes place. The nucleus is surrounded by the nuclear envelope that is composed of a double membrane with pores having diameters of 9 nm. This nuclear envelope is a highly selective barrier that allows only a passive diffusion for molecules or particles having a size smaller than that of nuclear pores. Larger molecules are actively imported to the nucleus. This requires the use of a nuclear localisation signal (NLS), a cationic consensus peptide sequence that is recognised by nuclear machinery import complex proteins. In addition to these intracellular barriers, pDNA injected systemically needs to get over the extracellular barriers. It must be shielded in order to escape detection by the immune system. It must reach organs or tumours upon extravasation from the vascular lumen to the interstitial space through fenestrations or tight junctions of the endothelial layer or upon transcytosis *via* endothelial cells laying the blood vessels.

Altogether, the above mentioned processes show that the design of optimal targeted gene delivery systems based on chemical compounds is highly challenging. Besides

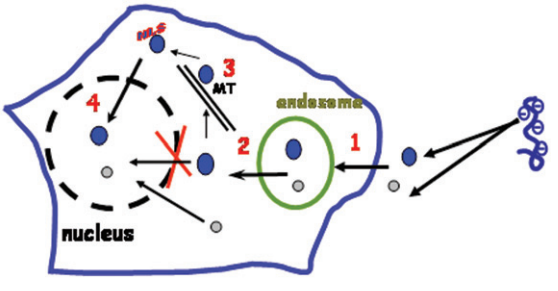

Figure 1. Intracellular barriers of gene delivery: (1) Plasma membrane; (2) endosomal escape; (3) cytosolic diffusion; (4): nuclear import. MT: microtubules or actin microfilaments constituting cytoskeleton architecture. The nucleus is delimited by a nuclear envelop with pores of 9 nm diameter. Small molecules (<40 kDa) (o) can diffuse passively through the nuclear pore while larger molecules (●) require the use of nuclear localisation signal (NLS).

chemical gene delivery systems, several physical methods starting from a simple naked DNA injection to much more sophisticated systems such as electroporation and USMD have been proposed. The latter seems to fulfil the requirements of a safe site-specific delivery by combining targeting and cell delivery of gene due to the possibility of focused microbubble activities by ultrasound insonation.

The ultrasound imaging community has seen dramatic technical advances over the last two decades. Today, ultrasound imaging is an established and confident technique for clinical diagnosis. Various advances in terms of equipment and signal processing have contributed to a better understanding of the anatomy and function of various organs. With the introduction of real-time two dimensional imaging, a variety of anatomical structures can be visualised non-invasively. Moreover, new ultrasound applications become possible with the introduction of important technological innovations. Real-time three dimensional imaging is now a reality with the availability of matrix array transducers containing more than 3000 elements, each of them the size of a human hair. With such two-dimensional array transducers, commercially available scanners are able to provide real-time volumetric images with adequate resolution and image quality. The recent introduction of USCAs provided a major breakthrough and has brought a revolution in clinical US applications. It has stimulated production of a new class of imaging methods such as harmonic imaging, which is already evident in commercial systems.

Contrast imaging methods aim to identify and display the echo from the contrast agent and to reject the echo from the surrounding tissue, offering a new way for the detection of tissue microvasculature. US images reproduce echoes being reflected by the insonated structures (ultrasonic backscatter). Therefore increasing the amount of echo amplitudes from the insonated areas will boost the quality of the created ultrasonic image. This is definitely important when dealing with tiny vessels beyond the resolution of current ultrasound imaging equipment. As in MRI, CT, and conventional X-ray imaging modalities, the use of contrast agents could change the way US imaging is performed, opening novel and unique diagnostic opportunities.

USCAs are currently commercially available in Europe, Asia and United States. They consist of tiny gas microbubbles with a mean diameter of 3 μm, smaller than red blood cells and are therefore appropriate for intravenous injection. The microbubbles are stabilised by a shell of biocompatible material such as protein, lipid or polymer to extend their lifetime. Microbubbles display similar flow dynamics as blood and are ultimately metabolised from the blood pool [6].

Recently, new USCAs have been developed that are characterised by both a smaller mean size and a prolonged persistence. Various techniques have been used to combine materials that control the bubble shell and gases with low diffusion rates [6]. A widespread engagement of pharmaceutical companies to USCAs has been realised, leading to a number of commercially available contrast agents and others that are under development [6]. Table 1 displays examples of approved contrast agents and those clinically available. Sonovue™ is a second-generation contrast agent, composed of sulfur hexafluoride gas bubbles coated by a highly elastic phospholipid monolayer shell. The diameter of Sonovue™ bubbles ranges from 1 to 12 μm [7]. Sonovue™ has been approved and is now available in many European countries. Definity™ is another commercially available second-generation contrast agent. Resulting from a lipid-based technology, it consists of

Table 1. Currently approved and/or commercially available ultrasound contrast agents.

Manufacturer	Name	Gas	Shell	Status
Bracco	Sonovue	Sulfur hexafluoride	Phospholipids	Available EU
Dupont/BMS	Definity	Octafluoropropane	Liposome	AvailableUS
Mallinckrodt	Albunex	Air	Albumin	Available
Mallinckrodt	Optison	Octafluoropropane	Albumin	Available
Nycomed	Sonazoid	Perfuorocarbon	Lipid	Approved Japan
Point biomedical	Biosphere	Air	Bi-layer	Late clinical
Schering AG	Levovist	Air	Fatty-acid	Available

phospholipid-encapsulated microspheres containing octafluoropropane gas. Definity™ microspheres have a size range from 1.1 to 3.3 μm. They have recently been approved by the US Food and Drug Administration (FDA) for marketing in the USA and in a few countries of the European community under the Luminity™ trademark. Sonazoid™ microbubbles contain a perfluorocarbon gas stabilised by a surfactant and have a mean size of 3 μm. They are dedicated to applications in cardiology, and potentially radiology, including imaging of the heart and liver. Sonazoid™ has been recently approved in Japan for radiology.

2. Interaction of ultrasound waves and gas microbubbles

Contrast agents modify the acoustic properties of tissues and thus the behaviour of propagated ultrasound waves. The presence of gas microbubbles in the tissue induces various changes including an increase of the backscattered ultrasound wave amplitude, an attenuation of the ultrasound beam and a reduction of sound speed [6]. The relevant characteristics of ultrasound contrast agents are the amplification of the scattered ultrasound waves that can be split into passive and active processes. Microbubbles reflect the incident wave passively, due to the acoustic impedance mismatch between the gas and the surrounding medium (tissue). In addition, microbubbles act as an active reflector and become a source of ultrasound. When hit by an ultrasound wave, microbubbles compress during the positive pressure cycle and expand during the negative pressure cycle. These oscillations depend on the applied acoustic pressure and transmitted frequency and are maximal when the incident frequency coincides with the natural or resonance frequency of the bubbles. This resonance phenomenon is very important since the backscattered echo signal from a resonant bubble increases dramatically. Moreover, a resonant microbubble becomes a source of nonlinear ultrasound signals indicating the presence of novel frequency components in the backscattered signal at multiples of the transmitted or fundamental frequency with the most dominant at 2 times the transmit frequency. Consequently, the acoustic behaviour of a gas microbubble can be separated into three acoustic regimes depending on the applied acoustic pressure and frequency. The mechanical index (MI) is an acoustic parameter that incorporates both variables. MI has been defined for safety purposes and is imposed by the Food and Drug Administration (FDA) to all ultrasound equipment manufacturers. MI expresses the quantity of mechanical work

supported by the microbubble during a single ultrasound cycle. It is defined as the ratio of peak negative pressure in mega pascal upon the square root of the incident frequency in megahertz

$$MI = \frac{P\text{-}[MPa]}{\sqrt{f[MHz]}}.$$

According to the recommendations of FDA, the mechanical index should not exceed 1.9 in all clinically approved ultrasound scanners.

For low MI, microbubble compression and expansion are symmetrical with weak amplitudes. The microbubble size varies linearly with the acoustic pressure. For slightly higher MI, microbubble oscillation becomes asymmetric since its compression is smaller than its expansion. Microbubble asymmetric behaviour during compression and expansion is the source of nonlinear oscillations which are characterised by the generation of nonlinear frequency components, called harmonics (Figure 2). For much higher MIs, the microbubble breaks. Microbubble destruction depends strongly on the type of contrast agent and mainly the shell surrounding the gas. During microbubble destruction, the gas often escapes and forms novel free gas microbubbles that become sources of strong nonlinear frequency components [8].

Figure 3 shows the three acoustic regimes of the microbubble when the mechanical index is increased. For small MI, microbubbles oscillate linearly and provide significant amplification of the echo signal, mainly in Doppler applications where large vessels are investigated. This behaviour corresponds to fundamental or conventional imaging modes which nowadays are rarely used for contrast imaging. For medium MI, microbubbles oscillate nonlinearly generating harmonic frequencies. The second harmonic frequency is currently used for contrast specific imaging and has become

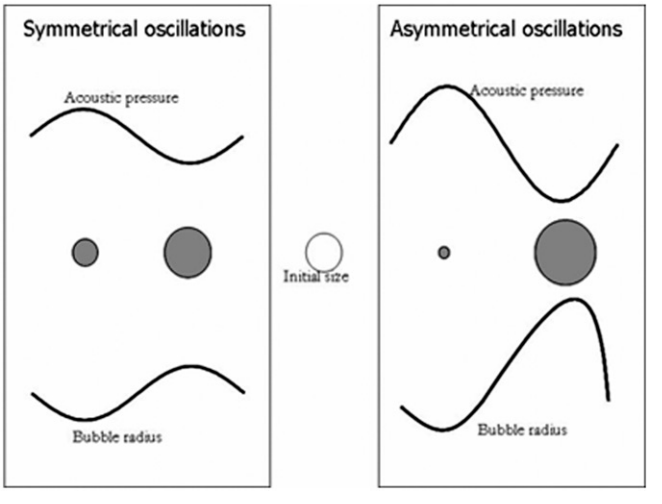

Figure 2. Symmetrical (linear) and asymmetrical (nonlinear) oscillations of a gas bubble under ultrasound activation.

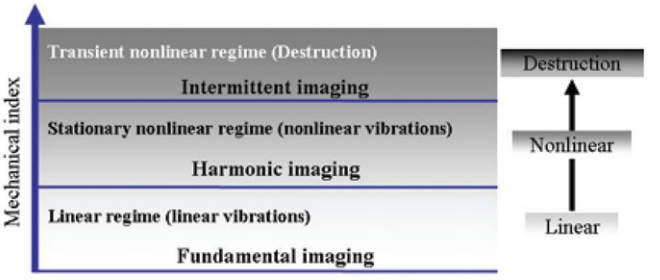

Figure 3. Three microbubbles acoustic regimes as a function of applied mechanical index.

a default imaging mode for contrast agents. Various imaging methods that exploit the second harmonic component have been proposed and are now implemented on recent ultrasound scanners. These include pulse inversion, power modulation and contrast pulse sequence [9]. When the MI is increased further, microbubbles are destroyed. This destruction is associated with the generation of transient but strong nonlinear frequency components. Triggered or intermittent imaging is a new imaging technique designed for contrast agent and operates only in the destructive mode.

3. Sonoporation-assisted gene delivery

It was quickly recognised that USCAs could play a role in therapy if used as vehicles for delivering drugs. The sonoporation phenomenon, thought to support drug delivery *via* a combination of microbubbles and US, is currently under investigation for a better understanding. This mechanism has been exploited for various purposes including gene transfer. The commercial availability of USCAs and the versatility of their use as well as their approval for clinical applications render USCAs-mediated gene delivery very attractive.

Over the last few years, several studies have demonstrated that under US insonation, microbubbles are able to modulate transiently the cell membrane permeability, thereby allowing molecules to be incorporated into cells [9]. Furthermore, the shells of microbubbles can be loaded with drugs or genes or functionalised by specific antibodies or ligands to target specific tissues [10].

Efficient sonoporation has been obtained with transmitted US frequencies close to those used clinically and extend from 0.5 to 4 MHz. Different molecules with variable molecular weights ranging from plasmids, oligodeoxynucleotide [11], and radioactive tracers [12] have been incorporated into cells by sonoporation. Plasmids encoding reporter genes as those of green fluorescent protein (GFP), luciferase or β-galactosidase are commonly employed as tools to monitor transfection efficiency. Figure 4 shows an example of sonoporation-mediated gene delivery into the human glioblastoma cell line (U87-MG) upon exposure to 1 MHz US at 310 kPa in the presence of perfluocarbone gas containing phospholipids bubbles (BRIU®, Bracco Research, Geneva) and a plasmid DNA encoding GFP gene. The green fluorescence staining corresponds to GFP expressed in the cytoplasm and in the nucleus.

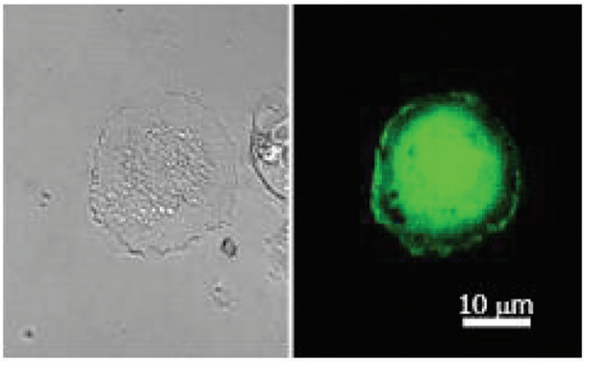

Figure 4. Confocal microscopy photograph of sonoporated human glioblastoma (U87-MG) cells. Cells were treated with plasmid encoding GFP gene in the presence of BRIU® microbubbles (20 bubbles per cell) and insonate during 1 min at 1 MHz, 310 kPa and 40% DC. (Right) GFP image; (left) phase contrast image.

4. *In vitro* US assisted gene delivery

The growing literature concerning sonoporation shows the potential interest of this method. Several cell types including cancer and primary cells have been tested to introduce plasmid DNA encoding reporter genes or fluorescent tracers as fluorescein-tagged dextran (Table 2 [13–22]). One can note that sonoporation is efficient even in endothelial and smooth muscle cells that are known to be resistant to conventional transfection methods such as lipofection. However, the efficiency is highly dependent on the cell type, although this could be attributed to different experimental set-ups used in these reports. Indeed, US parameters applied were variable in terms of frequency (from 1 to 3 MHz), of acoustic power (from 0.5 to 2W/cm^2) and insonation (exposure) times ranging from 10 sec to 30 min. These parameters influence considerably the efficacy of the delivery. The combination of US with gas microbubbles is required to get an optimal delivery even though application of US alone was shown to induce a weak molecular transfer into cells [14]. While it is difficult to make direct comparison between the data reported in Table 2, it seems that transfections with a 1 MHz frequency are the most efficient. The results also point out differences between the cell loading efficiency (percentage of FITC dextran-positive cells) and the gene delivery efficacy (percentage of GFP positive cells or luciferase activity). For example, sonoporation of MATBIII cells under 2.25 MHz, 507 kPa and Bracco's USCAs allowed the loading of 60% cells with FITC-dextran, but only 20% of them expressed GFP when they were transfected with a plasmid encoding GFP gene.

Microbubble stability is considered a critical parameter [22] in sonoporation. A positive correlation between USCA life time and sonoporation efficiency has been demonstrated. Microbubble stability is dependent, in part, on gas composition. A comparison between air filled microbubbles (Levovist® and Albunex®) and octafluoropropane gas bubbles (Optison®) has shown that the transfection efficiency of CHO cells with Optison® was 7-fold higher than with the other bubbles at 1 MHz, 20% duty cycle (DC) and 0.5 W/cm^2 [22]. As most other delivery methods, USMD can affect cell viability. In most *in vitro* studies such as those shown in Table 2, the toxicity

Table 2. Summary of *in-vitro* sonoporation studies.

Ref.	Cell type	Frequency	Acoustic pressure	Exposure time	Bubble type	Marker	Incorporatuin rate–transfection rate	Toxicity
[13]	Adherent TrampC2 prostate cancer cell line (Pca)	1 MHz	2 W/cm^2	30 min	Optison®	pGFP	47% of transfected cells	Viability higher than 75%
[14]	Endothelial (EC) and vascular smooth muscle cells (VSMC)		2,5 W/cm^2	1 min	Optison®	pLuciferase	8000 and 7000 fold increase of gene expression comparatively to to luciferase activity obtained with naked DNA alone in EC and VSMC, respectively	No apparent cell toxicity induced by ultrasound and Optison® determined by LDH activity measurement
[15]	Mammary adenocarcinoma cells (MATBIII)	2.25 MHz	507 kPa	10 sec	Phospholipid and perfluorocarbon microbubble (Bracco Research) 25–30 bubbles per cell	pGFP	20% of transfected cells	Marker: propidium iodide Viability: 85–94%
[16]	Human immortalised chondrocytes	1 MHz	400 kPa	20 sec	Albunex®	pGFP	50% of transfected cells	Not determined
[17]	Porcine aortic smooth muscle cells	1 MHz	2 MI or 128 W/cm^2	1 min	Albunex® 10% v/v or Optison® 10% v/v	pLuciferase	300 fold increase of luciferase activity comparing to naked DNA alone	Significant enhancement of H_20_2 release in presence of microbubbles
[18]	Baby hamster kidney (BHK-21)	1 MHz	2 W/cm^2	30 min	Optison® 10% v/v	pGFP	45% of transfected cells	Viability higher than 80%
[19]	Human epidermoid carcinoma cells (A 434)	1.5 MHz	2,3 MPa	75 sec	Optison® 2% v/v	pGFP	3,7% of transfected cells	Viability: 96,6%
[20]	Human umbilical vein endothelial cells (HUVEC)	1.9 MHz	80 mW/cm^2	5 min	Sonovue®	pGFP	16% of transfected cells	Marker: blue trypan Viability: 91%
[21]	Chinese hamster ovarian cells (CHO)	1 MHz	0.5-1 W/cm^2	20 sec	Optison® 2% v/v	pGFP	35% of transfected cells	Viability: 62%

induced by this technique is rather low compared to other transfection reagents or methods that can induce up to 50% of cell mortality depending on the cell type. To optimise the sonoporation efficiency, various US parameters and USCA concentrations have been evaluated on human U87-MG glioblastoma cells. Sonoporation efficacy was particularly correlated to the acoustic pressure [17], to duty cycle [23,24] and to the total exposure time [23,24]. In Figure 5 is an example of the duty cycle influence on the sonoporation efficiency of U87-MG cells performed at 1 MHz and 310 kPa with BRIU® microbubbles (20 microbubbles per cell) and a plasmid encoding GFP. The number of cells expressing GFP varied with DC and reached approximately 40% at DC of 40%. Cell viability was also correlated to DC and the percentage of cell death induced at 75% DC was twice as much as that obtained at 40% DC (40% versus 20%). In addition, the transfection efficiency was also dependent on exposure time (Figure 6). Two minutes of insonation led to a transfection rate of 43% which is about 10% higher than the rate achieved with 1 min insonation. This increase of the transfection efficiency did not induce higher cell mortality. In addition, the type of microbubbles, their lifetime [22] and their concentration, all have an impact on the sonoporation efficiency [17–23].

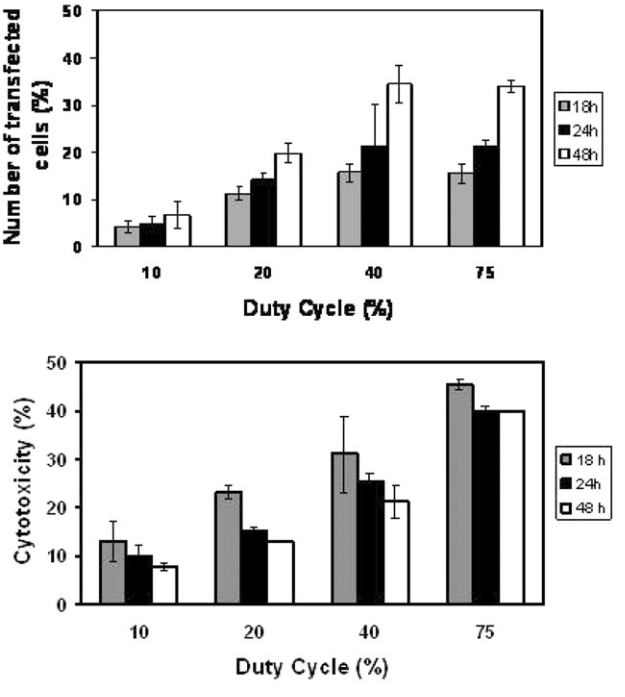

Figure 5. Duty cycle influence on the transfection efficiency rate. U87-MG cells were insonated during 1 min at 1 MHz, 310 kPa. Cells expressing GFP and dead cells were quantified by flow cytometry. Upper panel: Transfection rate; Lower panel: Cytotoxicity. Data shown are obtained relatively to the number of non-treated cells taken as 100%.

5. *In vivo* sonoporation assisted gene delivery

The majority of *in vivo* sonoporation studies have been conducted on rodent models. Different types of accessible organs have been tested largely due to developments and miniaturisation of ultrasound transducers. Tables 3 [25–30] and 4 [14,31–37] summarise *in vivo* sonoporation experiments that have been reported. The cardiovascular system was one of the first targeted systems that have aroused a real therapeutic perspectives for sonoporation. US in association with microbubbles have allowed both detailed visualisations of heart structures and gene delivery. Commercial and custom USCAs have been tested for their potential to deliver the luciferase gene in the left ventricle of rat hearts [33]. Using a triggered mode where one US insonation at 1.3 MHz was transmitted every four heart beats, gene expression was higher than with the continuous mode that induced extensive microbubble destruction. Moreover, the gene expression was restricted mainly to the targeted region (heart) with only a weak expression in other organs validating the targeted delivery of the method. It is worth mentioning that the safety of the method is excellent since no significant modification in host genes regulation has been reported. Another example that validates the utility of the method has been reported by Taniyama *et al.* on rat restenosis after angioplasty model [14]. Usually, the long term therapeutic effect of angioplasty is limited by restenosis occurring in 40% of patients due to an abnormal smooth muscle cell proliferation of intima. An overexpression of p53 protein in smooth muscle cells upon

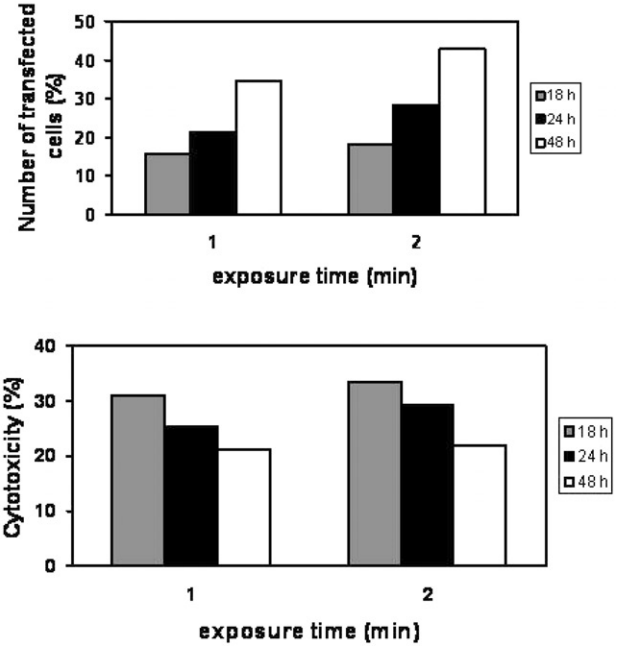

Figure 6. Influence of US exposure time on the transfection efficiency. U87-MG cells were insonated with similar US parameters as in Figure 4. GFP expressing cells and the rate of cell mortality were evaluated by flow cytometry. Upper panel: transfection rate; lower panel: cytotoxicity. Data shown are obtained relatively to the number of non-treated cells taken as 100%.

Table 3. Summary of *in-vivo* sonoporation studies.

Ref.	Organ/tissue	Frequency	Acoustic pressure	Exposure time to US	Bubble type	Marker/Therapeutical protein	Level of incorporation	Toxicity/Bioeffects
[25]	Rat myocardium	1.3 MHz	MI = 1.5	4 frames every 4 cardiac cycles	Perfluocarbon gas albumin coated microbubbles	pluciferase (4 mg/ml)	Specific luciferase activity detected up to 4 days only in heart	Not described
[26]	Coronary artery	1 MHz	2 W/cm^2	1 min	BR14®	GFP-siRNA (25 μg/ml)	Reduced GFP expression in coronary artery wall on GFP transgenic mice upon 48 h post-treatment	Arrhythmia observed after US exposure correlated with a prolongation of QRS complex. Heart rate recovered to baseline 2 min after the end of insonation
[27]	Sapheneous vein (*ex vivo*)	1 MHz	1.8 W/cm^2	2 min	Optison®	FITC tagged-oligonucleotides (4–5 μM)	High diffusion of FITC tagged-oligonucleotides in adventitial cells of saphein veins	
[28]	Rat myocardium	1.3 MHz	1.8 MPa	9 min	Perfluorocarbon-enhanced sonicated dextrose albumin (PESDA)	Mixture of 30 nm green fluorescent and 100 nm blue or red fluorescent nanospheres,	Nanoparticules delivery to the rat myocardium through microvessels rupture sites 4.8% of fluorescent tissues	Transient increase of heart rate

(*continued*)

Table 3. Continued.

Ref.	Organ/tissue	Frequency	Acoustic pressure	Exposure time to US	Bubble type	Marker/Therapeutical protein	Level of incorporation	Toxicity/Bioeffects
[13]	Prostatic adenocarcinoma subcutaneously induced in mice	1 MHz	2 W/cm^2	20 min	Optison®	pluciferase (100 µg)	Significant increase of lucificerase activity with Optison® comparing to ultrasound alone detected into tumour	Increase of intratumoural temperature
[29]	Tibialis anterior muscle transfection in mice	1 MHz	2 W/cm^2	30 sec	Optison® Sonovue® Levovist®	pGFP (330 µg/ml)	A best transfection rate was obtained with Optison® in comparison with Sonovue® and Levovist® microbubbles	A slight increase of damaged tissue and protective effect of Optison® in comparison to Levovist®
[30]	Direct injection into the striatum and the cisterna magna of mice brain	1 MHz	5 W/cm^2	10 sec	Optison®	luciferase (2 mg/ml)	Luciferase activity was increased in presence of Optison® in cisternal and striatal regions after 4 and 14 days respectively	No blood brain barrier disruption observed A transient hemorrhagic bleeding at the injection site that was not enhanced with microbubble presence

sonoporation with p53 anti-oncogene gene in the presence of US (2.5 W/cm^2) and Optison® microbubbles has led to an inhibition of intima cells proliferation on rat carotid artery after angioplasty [14]. This strategy could be used as a preventive treatment for patients after angioplasty. Brain diseases could also be treated with US-enhanced gene delivery. There are several reports concerning *in vitro* gene delivery into neural cells and the use of US to breach the blood brain barrier [10,38,39]. It has been shown that transcranial application of ultrasound at 2.20 MHz and 0.57 MPa associated with an intravascular injection of Optison® microbubbles can reversibly permeabilise the blood brain barrier in rabbit. Therefore, the central nervous system known to be rather inaccessible to therapeutic agent can be breached upon sonoporation. This method has also permitted an increase of blood capillary permeability in skeletal muscles [40, 41]. In another study, Song has shown extravasation of microspheres from blood vessels and their transfer into skeletal muscle tissue at 1 MHz and 0.75 MPa in the presence of Optison®. Another report relates the injection of pDNA encoding luciferase gene combined with cationic lipid microbubbles by intra-muscular (IM), intra-venous (IV) or intra-arterial (IA) routes and with an insonation of rat hind limb skeletal muscles [41]. The luciferase activity detected in limb muscles following IA injection was similar to that obtained following IM and was 200-fold greater than that achieved after IV administration. These results indicate that insonation away from injection site can induce sufficient extravasation of pDNA to transfect muscles. The feasibility of using USMD has also been examined for mammary carcinoma [42], and prostate cancer [28]. In a rat tumour model obtained by implantation of mammary carcinoma cells in adipose tissue, experimental microbubbles and plasmid injected directly into tumour followed by insonation led to an efficient gene expression without causing inflammatory response or necrosis [42]. In a murine PCa prostate cancer model, sonoporation with 1 MHz transducer, 2 W/cm^2 and 30% DC applied for 20 or 30 min in the presence of Optison® induced a 2-fold increase of gene expression compared to pDNA alone [28]. In a separate study Hauff has demonstrated that 50% reduction of pancreas adenocarcinoma tumour growth can be obtained after three intra-tumoural administrations of plasmid encoding p16 combined with US (color Doppler mode, MI = 1.5) and microbubbles [43]. Recently, a significant effect has been reported on gingival squamous carcinoma cells implanted in nude mice [44]. A complete suppression of tumour growth was obtained in mice transfected with Optison® and plasmid encoding cytolethal bacterial toxin A using a transducer of 1 MHz with an output of 2W/cm^2 and 50% DC. Altogether, these results indicate that selective US conditions offer the possibility to transfer therapeutic genes in various tissues. However, data reported in Tables 2 and 3 show that the sonoporation efficiency is highly dependent on the US parameters, the USCA properties and the type of cells or tissues under investigation. Few *in vivo* studies in mice, rat and porcine models using reporter and therapeutic genes have been carried out to assess the effectiveness of USMD (Tables 3 and 4). Therapeutic genes and microbubbles were injected either intravenously or directly into the tissue of interest. The results showed that the USMD induced a significant improvement in gene delivery compared to injection of pDNA alone. When reported, the toxicity of the treatment seemed to be mild or insignificant despite the large amounts of pDNA used (more than 1mg).

Table 4. Selection of *in vivo* sonoporation studies using therapeutic genes.

Réf.	Organ/tissue	Transmit frequency	Acoustic pressure	Exposure time to US	Bubble type	Therapeutic gene	Level of incorporation/therapeutic effect	Toxicity/Bioeffects
[14]	Restenosis after angioplasty model induced in rat carotid		2.5 W/cm^2	2 min	Optison®	p53 (250 μg)	A significant inhibition of neointimal-to-medial area ratio 2 weeks post-transfection	Not described
[31]	Human hepatocellular carcinoma cells	1 MHZ	2 W/cm^2	10 min	BR14®	INFβ Subcutaneous intratumour injection (50 μg)	At 6 weeks post-treatment, decrease by 70% of tumour growth in treated mice comparatively to control miceAbsence of metastasis 12 weeks post-treatment	No apparent lesions induced by US and/or microbubble treatment
[32]	Rat acute myocardial infarction model	1,3 MHz	MI = 1.1	2–4 min min	Optison®	HGF (Hepatocyte Growth Factor)1mg/ml infused in the left ventricular chamber	Increase of capillary and arterial density in treated area of treated group. Significant reduction of ischemic area comparatively to control group	No difference in mortality of no US and controls
[33]	Rat pancreatic islets in the context of type 1 diabetes	1.3 MHz	MI = 1.2 – 1.4	20 min focused on pancreas	Phospholipid shell of perfluoropropane gas-filled microbubbles bearing the therapeutic gene	Human insulin and hexokinase (250 μg of plasmid associated with microbubblesIntravenous injection	A clear increase of circulating C- peptide and a decrease of blood glucose levels. These effects were correlated to an increase of insulin level in blood measured 5 and 10 days after treatment	No inflammation and necrosis

[34]	Rat myocardium	1.3 MHz	MI = 1.6		Lipid-stabilised microbubbles bearing the therapeutic gene	hVEGF (human vascular endothelial growth factor)(0.6 mg/kg)Intra-venous injection	Maximal expression of hVEGF in cardiac tissue 10 days after treatment. This expression was associated with an increase of myocardial capillary and arteriolar density	No alteration of the morphology and cardiac function
[35]	Liver of hemophilia B murine model	1.1 MHz	0.8 MPa-4 MPa	1 min	Optison®	Factor IX (5 μg by intrahepatic injection)	Increase of factor IX in blood samples and produced by the hepatocytes in comparison to control condition	Transient hepatic lesions appeared with a focal coagulation necrosis and haemorrhages in liver
[36]	Renal fibrosis in rat UUO (unilateral urethral obstruction) model	1 MHz		1 min	Optison®	Smad7: intracellular mediator an regulator of TGF-β signalling (50 μg/ml by renal arterial injection)	Reduction of collagen I and III mRNA and protein expression Inhibition of myofibroblasts tubuloinsterstial accumulation and tubular atrophy	No histological and functional changes were observed
[37]	Sapheneous vein in a porcine interposition graft model	1 MHz	MI = 1.8	1 min	BR14®	TIMP-3 (Tissue inhibitor of metalloproteinase 3) (33 μg/ml)	Significant increase of lumen size correlated to a reduction of neointimal-to- medial ratio area	Increased neointima formation induced by US alone

Overall, *in vivo* studies confirm the potentiality of USMD and with no doubt, gaining more insight into the sonoporation mechanism will further improve this gene delivery method.

6. Mechanisms of membrane permeabilisation

The mechanism(s) of molecular translocation into cells *via* sonoporation is not well understood. One likely hypothesis considers that the activities of microbubbles under ultrasound insonation are responsible for transient pore formation in the cell membrane. Marmottant and colleagues [45] have observed with a high speed camera the deformation of lipidic vesicle and release of their fluorescent content in contact with the microbubble. The release of the fluorescent marker was induced by a transient membrane rupture upon contact with oscillating microbubbles. Electrophysiological studies have shown that sonoporation induced a variation of potential membrane and transmembrane currents. Deng *et al* [46] demonstrated on Xenopus ovocyte that US in the presence of microbubbles transiently increases transmembrane currents induced by a decrease of the membrane resistance probably due to pore formation. The amplitude of the measured current is strongly dependent on the acoustic pressure and insonation time [46]. Recently, observations with a high speed camera have shown that interaction of microbubbles with cells led to variable effects [47]. For a low acoustic pressure, the microbubble–cells interaction has generated a mechanical compressive stress [47]. This membrane stimulation could be responsible for the permeability probably *via* pores formation allowing cellular entry of external molecules. Conversely, high acoustic pressures could produce bubbles destruction or violent acoustic phenomena such as microjets [48]. Microjetting is due to microbubble deformation under funnel shape that can be projected and directed to cell extremity. The projection speed can reach $100\,m\,s^{-1}$ creating a membrane disruption at the cell contact [48]. Microbubbles under the influence of US may also cause cell membrane deformation due to mechanical stress. Patch clamp exploration of electrophysiological properties of mammary cancer MDA-MB 231 cells has shown that sonoporation induces modifications in membrane potential by triggering stretch activated ionic channels [49]. Insonation of microbubbles in contact with the plasma cell membrane decreases instantaneously the membrane potential. It is worth noting that despite the induction of mechanical stresses through the microbubble oscillations, the cell viability was unaffected [49].

In order to validate the pore formation hypothesis and to determine pore size, the incorporation of nanoparticles with different sizes have been evaluated [15, 16]. Efficient transfer was achieved when the pore size was of the order 37 to 75 nm. Investigations on the transfer of a fluorescent plasmid DNA and its intracellular distribution during sonoporation have shown that plasmid DNA entry does not depend on the endocytosis pathway which differs from transfection pathways as induced with DNA/cationic lipids (lipofection) or DNA/polymers (polyfection) complexes. During sonoporation, plasmid DNA was distributed homogeneously into the cytoplasm [16]. In contrast, plasmid DNA/cationic lipids complexes are confined inside endocytic vesicles from where the plasmid DNA must escape to enter the nucleus to be expressed [16]. The kinetics of gene expression after sonoporation and lipofection has been investigated [12,15,16,50]. It appears that sonoporation allows transfer of plasmid DNA directly into the nucleus allowing a faster

expression of the green fluorescent protein than with lipofection. The latter involves slow and complex mechanisms for gene expression.

7. Electroporation

Electroporation involves the application of short high-voltage pulses to induce transient cell membrane permeabilisation thereby allowing the entry of extracellular molecules. Membrane destabilisation is achieved when the applied external electric field potential is above the plasma membrane potential. Membrane permeation is induced transiently when millisecond pulses of electric field are applied on cells in suspension but the cell viability is highly dependent on various parameters such as the field strength, pulse duration and number of pulses. Such electric pulses promote interaction of the plasma membrane with extracellular compounds favouring their progressive intracellular internalisation. It is generally accepted that gene transfer efficiency is related to a combination of membrane permeabilisation and DNA electrophoresis [51–53]. Five steps are now known to be involved in the kinetics of electropermeabilisation.

(1) Induction step (μs): the external electrical field induces an increase of membrane potential difference resulting in a local deformation when the value (critical permeabilisation threshold) reaches 200 mV. The magnitude of the defects is highly dependent on the buffer used.
(2) Expansion step (ms): the defects last as long as the field is maintained at an overcritical value.
(3) Stabilisation step (ms): a recovery of the membrane organisation as soon as the field is subcritical.
(4) Resealing step: the membrane reseals slowly on a scale of seconds or minutes.
(5) Memorial step: as a consequence of cell membrane modifications, membrane structural features (flip–flop) and some of its physiological features recover on a longer time scale.

A cell native transmembrane potential difference of 50–70 mV in magnitude is usually created by the difference in ionic strength between the intracellular and extracellular fluids. When exposed to an electric field, cells undergo different perturbations due to Joule heating and electromechanical effects (stretching and deformation which elevate the potential difference) (Figure 7). When this finally exceeds 200–300 mV, a structural rearrangement of the membrane occurs including lipid reorganisation and electroconformational change of proteins [54–56]. This threshold is highly homogeneous across different cell types [57,58], whereas the duration of electropermeation is dependent on the magnitude and the duration of the applied transmembrane potential [59,60]. Membrane temperature is an equally important factor since membrane physical properties are highly dependent on the temperature. The electric field creates pores, resulting in an increase of membrane electrical conductance and in short-circuiting transmembrane potential (ΔVm). Teissié and Tsong [61] have shown that 35% of pores induced by a strong field exposure of erythrocytes are linked to Na/K ATPase, ions channels. An electrical field of a single 4-ms pulse and 500 mV decreases Na^+ and K^+ channel currents by 20% and 30%, respectively. The kinetics of electroporation depend strongly on the voltage applied on the cell membrane

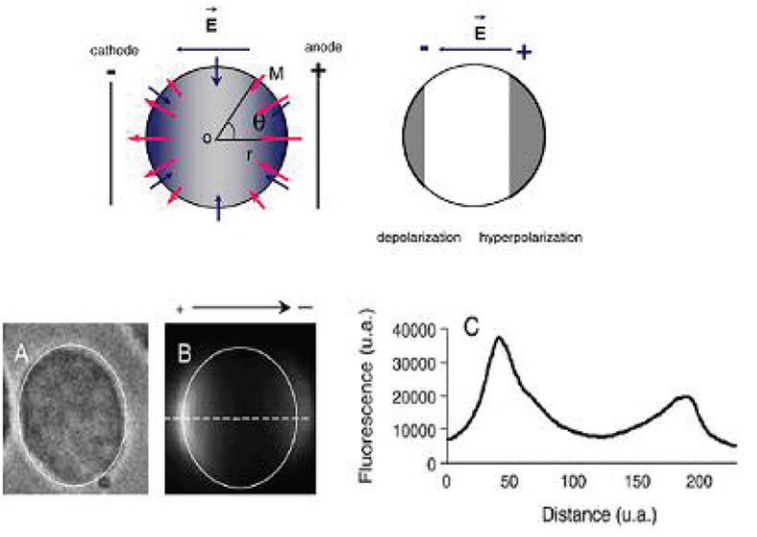

Figure 7. Modulation of electric potential difference of a cell by electrical field. The native transmembrane electrical potential difference $\Delta\psi E$ is superimposed by the one induced by the electrical field $\Delta\psi O$. Arrows are representative of electrical potential gradient directions (blue: resting potential; red: electrical field induced potential). Cell is hyperpolarised at its side facing the anode and depolarised at the other side facing the cathode; Visualisation of permeabilised cells following electroporation (8 pulses for 5 ms duration, 1Hz, 0.8 kV/cm) applied in the presence of propidium iodide. Images shown are obtained 1 s after the electropulsation, (A) phase contrast, (B) fluorescence and (C) fluorescence intensity radial profile along the dotted line. Black arrow corresponds to the electric field direction.(a.u: arbitrary units) (Adapted from [60], courtesy of M.P Rols and J. Teissie and with the permission of Elsevier).

Molecules with sizes less than 4 kDa have been directly introduced into the cytosol using electroporation. These workers found that such molecules could asymmetrically cross the membrane sides facing the 2 electrodes. It was found too that the membrane leaflet area facing the anode is more permeabilised than the leaflet area facing the cathode [51,60]. For larger molecules such as plasmid DNA, more complex steps are involved. For example, using fluorescence microscopy digitised imaging Teissié and co-workers were able to make observations of the first events at the single cell level. They observed that permeabilisation occurs at the cell membrane side facing the electrodes while molecular DNA interaction with the cell membrane occurs on the membrane leaflet facing the cathode. The DNA molecules are entrapped as clusters of 0.2 μm domains. The electric field induces interaction between electropermeabilised membrane and DNA molecules leading to its insertion. No free plasmid DNA diffusion into the cytoplasm was detected. The transfection efficiency increased from 20% to more than 40% when the polarity of the electrical pulses was inverted between each pulse, suggesting that changing pulse polarity or pulse direction leads to increased DNA/membrane interactions [62,63].

Taken together, the following conclusions can be drawn from these studies: (i) the electric field must be strong enough to induce the membrane destabilisation; (ii) DNA must be stable and present during the electroporation; and (iii) the electrical field pushes

DNA in the bulk towards the cell membrane. The transmembrane passage of such a big molecule is a post-pulsing event because it is very slow.

In vivo, it seems that a pool of DNA escapes from the attention of extracellular nucleases and can be electrotransfered successfully up to 4 hours [64]. A number of studies have demonstrated that, when applied, *in vivo* electrotransfer markedly enhances (100–1000 fold) gene expression compared to naked plasmid DNA injection into a variety of tissues such as skin, muscle, lung, tumours, synovium cartilage, cardiac muscle, brain, retina, cornea as well as spinal cord [65,66]. Moreover, it has been shown that electrically assisted gene delivery has potential to be used as therapeutic intervention in several diseases such as muscular dystrophy, cancer, arthritis and blood disorders [65,66]. Pulses can be exponential [67] or square [68] waves, their number varied from one to 14 with 100–300 μs to 50 ms of duration and the electric field strength can be high (1500 V) or low voltage (50 V). Successful *in vitro* and *in vivo* DNA delivery can be realised by application of high voltage with short pulses followed by a low voltage and long pulses duration to induce DNA electrophoresis. Therefore, optimisation of the procedures is of importance for each application. The type of electrode and the distribution of electrical field inside the tissue are two major parameters. The electrode configuration governs the field distribution in tissues, and that in turn controls the effectiveness of the electropermeabilisation [69]. Plate electrodes are widely used for muscle and tumour electroporation. This is because they allow transcutaneous application of pulses with a homogenous electric field. Conversely, a high field voltages need to be applied in order to reach the threshold value for permeabilisation although these voltages can cause electrical skin burns as well as necrosis or apoptosis of underlying tissues. Needle electrodes allows for a deeper penetration inside tissues but cause heterogeneity of the electrical field distribution that is higher near the needles and on their tips, causing local damage. New types of electrodes have been designed to overcome the limiting effect of the formers. Amongst them are meander contact electrodes [70,71], syringe electrode devices that allow for simultaneous injection of DNA and application of electric field [72], spatula electrodes [73] and needle-free patch electrodes [74].

8. Sonoporation assisted-gene delivery improvements

As in electroporation, sonoporation induces a membrane destabilisation leading to increased DNA incorporation. These two methods induce a hyperpolarisation of the plasma membrane due to activations of ionic channels upon mechanical stress [49]. Whereas initial electroporation procedures caused considerable cell damage, developments over the past decades have led to unprecedented levels of equipment sophistication and protocol optimisations that have reduced these drawbacks. Nowadays, sonoporation seems to induce minimal cell damage. In order to improve its efficiency and hasten its clinical acceptance, improved knowledge of the mechanism(s) will be of importance. Having a clear understanding of the influence of US parameters in terms of transducer type, output power and the pulse sequencing mode on microbubble activities will be crucial for improvement. This will likely require the design of new types of transducers, determining the pulse number, the acoustic frequency and power. Most importantly, the type of gas and the bubble shell compositions that best mediates bubble stability and their

use are crucial for microbubble formulation. Similarly, knowledge of the relationship between the optimal bubble size and ultrasonic frequencies that mediate gene delivery will likely improve the technology.

Sonoporation offers the possibility of combining imaging and targeted gene delivery. The design of a new multi-frequency transducer could be useful because frequencies available for imaging on most US scanners are not optimal for gene delivery. It is also thought that developing implantable miniature ultrasonic devices operating over months or days that can be implanted near or inside the tumour *via* a percutaneous needle insertion [75] will have a significant therapeutic contribution. This technique will be suitable for localised cancers that may not be resectable such as prostate cancers which do not respond to radiotherapy.

9. Nanobubble development

Most available USCA exhibiting size ranges from 1–10 μm are relatively large compared to traditional pharmaceutical vehicles. One challenge is to reduce the bubble size at submicron scale to gain a powerful targeting function. Indeed, targeting of cells outside capillaries requires bubbles with a size less than 1 μm, facilitating their extravasation through endothelium of blood vessel. The 'leaky' tumour vasculature presents pores with cut-off size between 380 nm and 780 nm [76,77]. To date, few studies on the development of nanoscale size USCA have been reported. For this purpose, nanoemulsions or nanodroplets containing liquid perfluorocarbon have been synthesised [78,79]. These particles are 10 fold smaller and more stable than microbubbles under pressure and mechanical stress. Although they exhibit low echogenicity in solution, it is highly increased once they are deposited on a monolayer. So, these nanoparticles will be only detectable once adhered to their target site. Dayton *et al.* [79] have reported that application of US with high duty cycle pulses can deflect such perfluorocarbon nanodroplets in the acoustic field due to their displacement in the direction of US propagation. US application appears to concentrate these nanoparticles on a cell monolayer and a maximal effect is obtained at 5 MHz with an intensity of 2.4 W/cm^2. Because they do not exhibit large radial oscillations as USCA microbubbles, these nanoparticles remain intact after application of high acoustic pressure in the order of magnitude of MPa (3 MPa at 10 MHz). So, the drug release inside the targeted cell could not be obtained *via* a sonoporation effect. Still, such small USCAs can be used as specific targeted contrast and delivery vehicles that can act through non-destructive mechanisms.

Recently, a very elegant approach consisting of preparing mixtures of drug-loaded polymeric micelles and perfluoropentane nano/microbubbles stabilised by biodegradable block copolymer has been proposed [80]. In this system, phase state and nanoparticle sizes are sensitive to the copolymer/perfluorocarbon volume ratio. Doxorubicin-loaded nanobubbles were able to extravasate selectively into the tumour interstitium, upon intravenous injection in mice. These nanobubbles coalesced to produce microbubbles with a strong, durable ultrasound contrast. The nascent microbubbles oscillated and collapsed under the action of tumour-directed ultrasound enhancing significantly drug uptake by tumour cells *in vitro*. A tumour regression in the mouse model was observed in mice treated with these nano/microbubbles loaded with doxorubicin.

In conclusion, the development of submicron USCAs deserves attention for their promise in targeted therapy and imaging. Nevertheless the development of a more appropriate ultrasound technology could be required to exploit such nanobubbles.

10. Conclusions

Sonoporation constitutes a transfer method with low toxicity, easy to implement, adaptable to different cell types and suitable for *in vivo* situations. However, membrane permeabilisation and penetration mechanisms should be clarified to improve molecule incorporation. Sonoporation seems to be a delivery technique that provides efficient gene transfer with safety for healthy tissues. Moreover, it offers the possibility to associate ultrasound imaging and therapy. Loading bubbles with specific antibodies and focusing the US beam in a limited organ area will achieve a targeted therapy. Indeed, both accumulation of therapeutic agent contained-targeted bubbles and induction of membrane permeability through interaction of oscillating bubbles with cell surface will increase cellular incorporation of therapeutic agents.

References

[1] S.E. Raper et al., *Fatal systemic inflammatory response syndrome in a ornithine transcarbamylase deficient patient following adenoviral gene transfer*, Mol. Genet. Metab. 80 (2003), pp. 148–158.
[2] S. Hacein-Bey-Abina et al., *A serious adverse event after successful gene therapy for X-linked severe combined immunodeficiency*, N. Engl. J. Med. 348 (2003), pp. 255–256.
[3] S. Hacein-Bey-Abina et al., *LMO2-associated clonal T cell proliferation in two patients after gene therapy for SCID-X1*, Science 302 (2003), pp. 415–419.
[4] A.P. Rolland, *From genes to gene medicines: recent advances in nonviral gene delivery*, Crit. Rev. Ther. Drug. Carrier Syst. 15 (1998), pp. 143–198.
[5] R.I. Mahato, *Non-viral peptide-based approaches to gene delivery*, J. Drug Target. 7 (1999), pp. 249–268.
[6] A. Bouakaz and N. de Jong, *WFUMB safety symposium on echo-contrast agents: nature and types of ultrasound contrast agents*, Ultrasound Med. Biol. 33 (2007), pp. 187–196.
[7] M. Schneider et al., *BR1: a new ultrasonographic contrast agent based on sulfur hexafluoride-filled microbubbles*, Invest. Radiol. 30 (1995), pp. 451–457.
[8] A. Bouakaz, M. Versluis, and N. de Jong, *High-speed optical observations of contrast agent destruction*, Ultrasound Med. Biol. 31 (2005), pp. 391–399.
[9] D. Simpson, C. Chin, and P. Burns, *Pulse inversion Doppler: a new method for detecting nonlinear echoes from microbubble contrast agents*, IEEE Trans. Ultrason. Ferr. Freq. Con. 46 (1999), pp. 372–382.
[10] E.C. Unger et al., *Therapeutic applications of lipid-coated microbubbles*, Adv. Drug. Deliv. Rev. 56 (2004), pp. 1291–314.
[11] P. Haag et al., *Microbubble-enhanced ultrasound to deliver an antisense oligodeoxynucleotide targeting the human androgen receptor into prostate tumours*, J. Steroid. Biochem. Mol. Biol. 102 (2006), pp. 103–113.
[12] A. Van Wamel et al., *Radionuclide tumour therapy with ultrasound contrast microbubbles*, Ultrasonics 42 (2004), pp. 903–906.
[13] M. Duvshani-Eshet and M. Machluf, *Efficient transfection of tumors facilitated by long-term therapeutic ultrasound in combination with contrast agent: from in vitro to in vivo setting*, Cancer Gene Ther. 14 (2007), pp. 306–315.

[14] Y. Taniyama et al., *Local delivery of plasmid DNA into rat carotid artery using ultrasound*, Circulation 105 (2002), pp. 1233–1239.
[15] S. Mehier-Humbert et al., *Ultrasound-mediated gene delivery: kinetics of plasmid internalisation and gene expression*, J. Control Release 104 (2005), pp. 203–211.
[16] ——, *Plasma membrane poration induced by ultrasound exposure: implication for drug delivery*, J. Control Release 104 (2005), pp. 213–222.
[17] W.J. Greenleaf et al., *Artificial cavitation nuclei significantly enhance acoustically induced cell transfection*, Ultrasound Med. Biol. 24 (1998), pp. 587–595.
[18] A. Lawrie et al., *Microbubble-enhanced ultrasound for vascular gene delivery*, Gene Therapy 7 (2000), pp. 2023–2027.
[19] M. Duvshani-Eshet and M. Machluf, *Therapeutic ultrasound optimization for gene delivery: a key factor achieving nuclear DNA localisation*, J. Control Release 108 (2005), pp. 513–528.
[20] D.L. Miller, C. Dou, and J. Song, *DNA transfer and cell killing in epidermoid cells by diagnostic ultrasound activation of contrast agent gas bodies in vitro*, Ultrasound Med. Biol. 29 (2003), pp. 601–607.
[21] F. Nie et al., *Microbubble-enhanced ultrasound exposure improves gene transfer in vascular endothelial cells. World*, J. Gastroenterol 12 (2006), pp. 7508–7513.
[22] T. Li, K. Tachibana, and M. Kuroki, *Gene transfer with echo-enhanced contrast agents: comparison between Albunex, Optison, and Levovist in mice – initial results*, Radiology 229 (2003), pp. 423–428.
[23] K. Kaddur et al., *Optimizing ultrasound parameters for an efficient gene transfer in human glioblastoma cell line with BR14 gas microbubbles*. International Congress on Ultrasonics, (2007).
[24] S. Mehier-Humbert et al., *Ultrasound-mediated gene delivery: influence of contrast agent on transfection*, Bioconjug. Chem. 18 (2007), pp. 652–662.
[25] R. Bekeredjian et al., *Ultrasound targeted microbubble destruction can repeatedly direct highly specific plasmid expression to the heart*, Circulation 108 (2003), pp. 1022–1026.
[26] S. Tsunoda et al., *Sonoporation using microbubble BR14 promotes pDNA/siRNA transduction to murine heart*, Biochem. Biophys. Res. Commun. 336 (2005), pp. 118–127.
[27] T. Kodama et al., *Delivery of oligodeoxynucleotides into human saphenous veins and the adjunct effect of ultrasound and microbubbles*, Ultrasound Med. Biol. 31 (2005), pp. 1683–1691.
[28] D. Vancraeynest et al., *Myocardial delivery of colloid nanoparticles using ultrasound-targeted microbubble destruction*, Eur. Heart J. 27 (2006), pp. 237–245.
[29] X. Wang et al., *Gene transfer with microbubble ultrasound and plasmid DNA into skeletal muscle of mice: comparison between commercially available microbubble contrast agents*, Radiology 237 (2005), pp. 224–229.
[30] M. Shimamura et al., *Development of efficient plasmid DNA transfer into adult rat central nervous system using microbubble-enhanced ultrasound*, Gene Ther. 11 (2004), pp. 1532–1539.
[31] Y. Sakakima et al., *Gene therapy for hepatocellular carcinoma using sonoporation enhanced by contrast agents*, Cancer Gene Ther. 12 (2005), pp. 884–889.
[32] I. Kondo et al., *Treatment of acute myocardial infarction by hepatocyte growth factor gene transfer: the first demonstration of myocardial transfer of a 'functional' gene using ultrasonic microbubble destruction*, J. Am. Coll. Cardiol. 44 (2004), pp. 644–653.
[33] S. Chen et al., *Efficient gene delivery to pancreatic islets with ultrasonic microbubble destruction technology*, Proc. Natl. Acad. Sci. USA 103 (2006), pp. 8469–8474.
[34] G. Korpanty et al., *Targeting of VEGF-mediated angiogenesis to rat myocardium using ultrasonic destruction of microbubbles*, Gene Ther. 12 (2005), pp. 1305–1312.
[35] C.H. Miao et al., *Ultrasound enhances gene delivery of human factor IX plasmid*, Hum. Gene Ther. 16 (2005), pp. 893–905.
[36] H.Y. Lan et al., *Inhibition of renal fibrosis by gene transfer of inducible Smad7 using ultrasound-microbubble system in rat UUO model*, J. Am. Soc. Nephrol. 14 (2003), pp. 1535–1548.

[37] E.F. Akowuah et al., *Ultrasound-mediated delivery of TIMP-3 plasmid DNA into saphenous vein leads to increased lumen size in a porcine interposition graft model*, Gene Ther. 12 (2005), pp. 1154–1157.
[38] N. Sheikov et al., *Cellular mechanisms of the blood-brain barrier opening induced by ultrasound in presence of microbubbles*, Ultrasound Med. Biol. 30 (2004), pp. 979–989.
[39] K. Hynynen et al., *Non-invasive opening of BBB by focused ultrasound*, Acta Neurochir. Suppl. 86 (2003), pp. 555–558.
[40] J. Song et al., *Influence of injection site, microvascular pressure and ultrasound variables on microbubble-mediated delivery of microspheres to muscle*, J. Am. Coll. Cardiol. 39 (2002), pp. 726–731.
[41] D.L. Miller, S.V. Pislaru, and J.E. Greenleaf, *Sonoporation: mechanical DNA delivery by ultrasonic cavitation*, Somat. Cell Mol. Genet. 27 (2002), pp. 115–134.
[42] J.P. Christiansen et al., *Targeted tissue transfection with ultrasound destruction of plasmid-bearing cationic microbubbles*, Ultrasound Med. Biol. 29 (2003), pp. 1759–1767.
[43] P. Hauff et al., *Evaluation of gas-filled microparticles and sonoporation as gene delivery system: feasibility study in rodent tumor models*, Radiology 236 (2005), pp. 572–578.
[44] K. Iwanaga et al., *Local delivery system of cytotoxic agents to tumors by focused sonoporation*, Cancer Gene Ther. 14 (2007), pp. 354–363.
[45] P. Marmottant and S. Hilgenfeldt, *Controlled vesicle deformation and lysis by single oscillating bubbles*, Nature 423 (2003), pp. 153–156.
[46] C.X. Deng et al., *Ultrasound-induced cell membrane porosity*, Ultrasound Med. Biol. 30 (2004), pp. 519–526.
[47] A. Van Wamel et al., *Micromanipulation of endothelial cells: ultrasound–microbubble–cell interaction*, Ultrasound Med. Biol. 30 (2004), pp. 1255–1258.
[48] M. Postema et al., *High-speed photography during ultrasound illustrates potential therapeutic applications of microbubbles*, Med. Phys. 32 (2005), pp. 3707–3711.
[49] T.A. Tran et al., *Effect of ultrasound-activated microbubbles on the cell electrophysiological properties*, Ultrasound Med. Biol. 33 (2007), pp. 158–163.
[50] M. Duvshani-Eshet et al., *Therapeutic ultrasound-mediated DNA to cell and nucleus: bioeffects revealed by confocal and atomic force microscopy*, Gene Ther. 13 (2006), pp. 163–172.
[51] T.D. Xie and T.Y. Tsong, *Study of mechanisms of electric field-induced DNA transfection. Effects of DNA topology on surface binding, cell uptake, expression, and integration into host chromosomes of DNA in the mammalian cell*, Biophys. J. 65 (1993), pp. 1684–1689.
[52] J. Teissie and M.P. Rols, *Manipulation of cell cytoskeleton affects the lifetime of cell membrane electropermeabilisation*, Ann. N Y Acad. Sci. 720 (1994), pp. 98–110.
[53] P.G. de Gennes, *Passive entry of a DNA molecule into a small pore*, Proc. Natl. Acad. Sci. USA 96 (1999), pp. 7262–7264.
[54] E. Neumann et al., *Gene transfer into mouse lyoma cells by electroporation in high electric fields*, Embo. J. 1 (1982), pp. 841–845.
[55] J. Teissie et al., *Electropermeabilisation of cell membranes*, Adv. Drug. Deliv. Rev. 35 (1999), pp. 3–19.
[56] D.C. Chang, *A physical model of nerve axon. II: Action potential and excitation currents. Voltage-clamp studies of chemical driving forces of Na+ and K+ in squid giant axon*, Physiol. Chem. Phys. 11 (1979), pp. 263–288.
[57] R.W. Glaser et al., *Reversible electrical breakdown of lipid bilayers: formation and evolution of pores*, Biochim. Biophys. Acta 940 (1988), pp. 275–287.
[58] T.R. Gowrishankar, W. Chen, and R.C. Lee, *Non-linear microscale alterations in membrane transport by electropermeabilisation*, Ann. N Y Acad. Sci. 858 (1998), pp. 205–216.
[59] M. Bier et al., *Kinetics of sealing for transient electropores in isolated mammalian skeletal muscle cells*, Bioelectromagnetics 20 (1999), pp. 194–201.

[60] B. Gabriel and J. Teissie, *Direct observation in the millisecond time range of fluorescent molecule asymmetrical interaction with the electropermeabilised cell membrane*, Biophys. J. 73 (1997), pp. 2630–2637.
[61] J. Teissie and T.Y. Tsong, *Evidence of voltage-induced channel opening in Na/K ATPase of human erythrocyte membrane*, J Membr. Biol. 55 (1980), pp. 133–140.
[62] C. Faurie et al., *Cell and animal imaging of electrically mediated gene transfer*, DNA Cell Biol. 22 (2003), pp. 777–783.
[63] C. Faurie et al., *Effect of electric field vectoriality on electrically mediated gene delivery in mammalian cells*, Biochim. Biophys. Acta 1665 (2004), pp. 92–100.
[64] M.F. Bureau et al., *Intramuscular plasmid DNA electrotransfer: biodistribution and degradation*, Biochim. Biophys. Acta 1676 (2004), pp. 138–148.
[65] F. Andre and L.M. Mir, *DNA electrotransfer: its principles and an updated review of its therapeutic applications*, *Gene Ther*. 11 Suppl 1 (2004), pp. S33–42.
[66] D.J. Wells, *Gene therapy progress and prospects: electroporation and other physical methods*, Gene Ther. 11 (2004), pp. 1363–1369.
[67] A.V. Titomirov, S. Sukharev, and E. Kistanova, *In vivo electroporation and stable transformation of skin cells of newborn mice by plasmid DNA*, Biochim. Biophys. Acta 1088 (1991), pp. 131–134.
[68] T. Nishi et al., *High-efficiency in vivo gene transfer using intraarterial plasmid DNA injection following in vivo electroporation*, Cancer Res. 56 (1996), pp. 1050–1055.
[69] D. Miklavcic et al., *The importance of electric field distribution for effective in vivo electroporation of tissues*, Biophys. J. 74 (1998), pp. 2152–2158.
[70] L. Zhang et al., *Enhanced delivery of naked DNA to the skin by non-invasive in vivo electroporation*, Biochim. Biophys. Acta 1572 (2002), pp. 1–9.
[71] L. Zhang and D.P. Rabussay, *Clinical evaluation of safety and human tolerance of electrical sensation induced by electric fields with non-invasive electrodes*, Bioelectrochemistry 56 (2002), pp. 233–236.
[72] F. Liu and L. Huang, *A syringe electrode device for simultaneous injection of DNA and electrotransfer*, Mol. Ther. 5 (2002), pp. 323–328.
[73] M. Dona et al., *Functional in vivo gene transfer into the myofibers of adult skeletal muscle*, Biochem. Biophys. Res. Commun. 312 (2003), pp. 1132–1138.
[74] S. Babiuk et al., *Needle-free topical electroporation improves gene expression from plasmids administered in porcine skin*, Mol. Ther. 8 (2003), pp. 992–998.
[75] T. Siu, R. Rohling, and M. Chiao, *Microdevice-based delivery of gene products using sonoporation*, Biomed. Microdevices. 9 (2007), pp. 295–300.
[76] R. Pasqualini, W. Arap, and D. McDonald, *Probing the structural and molecular diversity of tumor vasculature*, Trends Mol. Med. 8 (2002), pp. 563–571.
[77] S.K. Hobbs et al., *Regulation of transport pathways in tumor vessels: role of tumor type and microenvironment*, Proc. Natl. Acad. Sci. USA 95 (1998), pp. 4607–4612.
[78] G.M. Lanza and S.A. Wickline, *Targeted ultrasonic contrast agents for molecular imaging and therapy*, Curr. Probl. Cardiol. 28 (2003), pp. 625–653.
[79] P.A. Dayton et al., *Application of ultrasound to selectively localize nanodroplets for targeted imaging and therapy*, Mol. Imaging. 5 (2006), pp. 160–174.
[80] N. Rapoport, Z. Gao, and A. Kennedy, *Multifunctional nanoparticles for combining ultrasonic tumor imaging and targeted chemotherapy*, J. Natl. Cancer Inst. 99 (2007), pp. 1095–1106.